

Research Article

Embodying rather than encoding: Towards developing a source-filter theory for undulation gait generation

Longchuan Li ^a, Shugen Ma ^{b,1}, Isao Tokuda ^c, Zaiyang Liu ^c, Zhenxuan Ma ^c, Yang Tian ^c, Shuai Kang ^{d,*}

^a College of Information Science and Technology, Beijing University of Chemical Technology, Beijing 100029, China

^b Thrust of Robotics and Autonomous Systems, The Hong Kong University of Science and Technology (Guangzhou), Guangzhou 511453, China

^c Graduate School of Science and Engineering, Ritsumeikan University, Kusatsu 525-8577, Japan

^d College of Mechanical and Electrical Engineering, Beijing University of Chemical Technology, Beijing 100029, China

ARTICLE INFO

Article history:

Received 30 April 2024

Revised 9 June 2024

Accepted 15 July 2024

Available online 20 July 2024

Keywords:

Undulation gait

Morphological computation

Embodiment

Robot locomotion

ABSTRACT

Biological undulation enables legless creatures to move naturally, and robustly in various environments. Consequently, many kinds of undulating robots have been developed. However, the fundamental mechanism of biological undulation gait generation has not yet been well explained, which hinders deepening the investigation and optimization of these robots. Towards developing a theory for explaining this biological behavior, which will further guide the design of artificial undulation systems, we propose a hypothesis based on both biological findings and previous robotics studies. To verify the hypothesis, we investigate embodied intelligence of undulation locomotion via a mechanical system. Through experimental study, we observe the phenomenon that undulation gait is a production of the source, which is the torque inputs, and the filter, which is the natural dynamics of the system. We further derive a general mathematical model and conduct morphological computation accordingly. From a simple model to a complicated system, our work explores the principles of undulation gait generation. Our findings significantly simplify the control system design of artificial undulating systems.

© 2024 The Author(s). Published by Elsevier B.V. on behalf of Shandong University. This is an open access article under the CC BY-NC-ND license (<http://creativecommons.org/licenses/by-nc-nd/4.0/>).

1. Introduction

Undulation is the most common locomotion style for legless creatures. As observed from organisms with different body sizes and traveling in various environments [1], such a sinusoidal trajectory is produced by agilely bending their bodies and moving through the media via anisotropy. For example, sperm cells travel in high-viscosity fluid [2], worms crawl on soil [3], snakes slither in sand [4], and eels swim in high-pressure fluid [5]. Inspired by this phenomenon, plenty of multi-link robots have been developed [6–10] to perform locomotion tasks on various of terrains. Despite the differences among their morphologies and application scenarios, the fundamental control frameworks of their gait generation method share the same mechanism: controlling all of the joints to track a group of predetermined sinusoidal waveforms with specified phase differences, *i.e.*, the serpenoid curves designed by Hirose [11].

Although this traditional method can generate robust artificial undulation gait, its redundancy has already been found. Ma has shown the possibility of enabling snake-like robots creeping forward using the serpenoid curves as open-loop input torques, where trajectory tracking is unnecessary [12]. Besides, Wang et al. have shown that by controlling only the head joint to follow a sinusoidal curve, other joints can also undulate the body with appropriately injected mechanical energy [13]. In addition, Chen et al. and Cao et al. have shown that the actuation on the tail joint is unnecessary for undulation generation either in fluid [14] or on the ground [15]. Moreover, Li et al. have shown that minimalistic input torques that effectively excite the system's natural dynamics can produce undulation gait conveniently [16]. These works removed the redundancy of artificial undulation gait generation from different points of view. However, a general theory that describes its essence is still lacking.

In the domain of acoustics, there is a famous model called source-filter theory for speech production [17–19]. As shown in the left panel of Fig. 1, (quasi) periodic air flow coming from the lungs induces vocal fold vibrations, where the source sounds are filtered by the vocal tract based on its morphology. Accordingly,

* Corresponding author.

E-mail address: kangshuai@buct.edu.cn (S. Kang).

¹ Given his role as Associate Editor of this journal, Shugen Ma had no involvement in the peer-review of this article and had no access to information regarding its peer-review. The article was handled by Prof. Yibin Li.

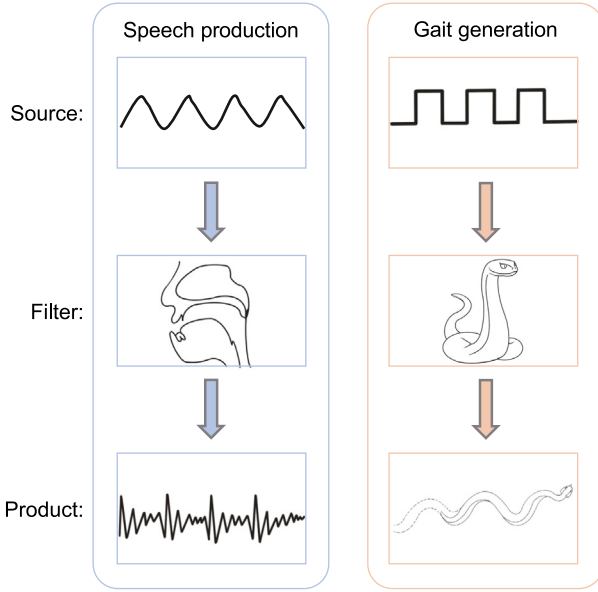


Fig. 1. Source-filter theory for speech production (blue color) and undulation gait generation (apricot color).

natural speech sound is produced. This theory not only well explains the natural speech production mechanism [20–22], but is also widely used for artificial speech synthesis [23–25].

Encouraged by the physical similarities between speech production and gait generation, where both of them articulate and create rhythmic patterns, we introduce a model in the right panel of Fig. 1, towards developing a source-filter theory for undulation gait generation. We hypothesize that undulation gait can emerge naturally without an intricate control framework if the morphology is well-designed and its dynamics are effectively excited. Accordingly, here the input torques created by muscles/motors are recognized as sources, the locomotion system is recognized as the filter, and the undulation gait is their product. This theory emphasizes that biological undulation is the product of simple inputs and elegant passive dynamics [26], rather than a complicated control system. Namely, biological undulation is embodied [27], rather than encoded. These statements are consistent with the biological findings that desert snakes robustly transit in heterogeneous environments with minimal sensing and control framework, benefiting from their passive muscle dynamics [28]. Moreover, the fact that vortex allows for passive swimming of dead fish [29] suggests that biological undulation generation relies more on its morphology, rather than the control. The theory developed in this work not only helps explain the biological process, but also suggests a new direction of artificial locomotion optimization, *i.e.*, refining morphology rather than control.

2. Phenomenon description

Using a mechanical system as a simplified model, Fig. 2 describes the experimental phenomenon of filtering behavior in undulation gait generation, where its detailed experimental setup can be found in the appendix. Fig. 2 (a) shows the experimental prototype machine of a 4-link locomotion robot. Each joint is actuated by a motor equipped on it, which corresponds to the source. Besides, a torsional spring is attached to the joint, which corresponds to the filter. This mechanical design is similar to Dear's work [30]. At the grounding points, anisotropic frictional forces along the normal and tangential directions can be guaranteed by passive wheels. Here, we compare two methods for undulation gait generation.

- (1) Common method: serpenoid curve tracking control.
- (2) Source filtering method: binary inputs injection.

According to the first method. The desired angular positions of the joints are shown in Fig. 2(b). Here, each joint strictly follows a predetermined sine wave, and the phase differences among them are $\frac{2\pi}{N-1}$. Here, $N = 4$ is the number of links. Accordingly, a smooth undulation gait is generated as shown in Fig. 2(c).

According to the second method. The robot does not need to track any predetermined trajectory. Instead, each joint is excited by a minimalistic torque, which is binary, as shown in Fig. 2(d). Besides, the phase differences among them are the same as the first method. Notably, a smooth undulation gait naturally emerges as shown in Fig. 2(e). To accomplish equivalent displacement, it takes more cycles compared to the first condition, which is due to the fact that its stride is smaller than it.

3. Modeling and analysis

3.1. Mathematical modeling

Here we derive a general mathematical model for the multi-link locomotion robot to analyze the phenomenon observed above. As shown in Fig. 3, the robot is composed of N identical links with the centralized mass of m . Besides, the length of the link is L , and the moment of inertia of it is \mathcal{I} . Define (x_1, y_1) as the center position of the first link counting from left, θ_j represents the angular position of each link with respect to the horizontal, where $j \in \mathbb{Z}^+$. Accordingly, the system dynamics can be described by a generalized coordinate vector $\mathbf{q} = [x_1 \ z_1 \ \theta_1 \ \dots \ \theta_j \ \dots \ \theta_N]^T$. The equation of motion of the robot reads:

$$\mathbf{M}\ddot{\mathbf{q}} + \mathbf{h} = \mathbf{f} + \mathbf{S}\mathbf{u} \quad (1)$$

where \mathbf{M} is the inertia matrix, \mathbf{h} is the combination of Coriolis and centrifugal forces (one can check [31] for the details). According to the principle of virtual work, the mechanical power of this multi-link locomotion system dissipated by frictions is calculated as follows:

$$\dot{\mathbf{E}}_f = -\sum_{j=1}^N (\dot{\mathbf{E}}_n + \dot{\mathbf{E}}_t) = \dot{\mathbf{q}}^T \mathbf{f} \quad (2)$$

where $\dot{\mathbf{E}}_n = v_{n_j} \mu_n \text{sign}(v_{n_j}) mg$, and $\dot{\mathbf{E}}_t = v_{t_j} \mu_t \text{sign}(v_{t_j}) mg$. Accordingly, \mathbf{f} can be derived, which is a vector that summarizes the vertical and horizontal frictions at each grounding point:

$$\mathbf{f} = -mg \times \sum_{j=1}^N \left(\mathbf{J}_{x_j}^T \mathbf{R}(\theta_j) \mu_n \text{sign}(v_{n_j}) + \mathbf{J}_{y_j}^T \mathbf{R}(\theta_j) \mu_t \text{sign}(v_{t_j}) \right) \quad (3)$$

Here, \mathbf{J}_{x_j} and \mathbf{J}_{y_j} are the Jacobian vectors that map the j th link velocities (v_{x_j}, v_{y_j}) to general velocities $\dot{\mathbf{q}}$. Besides, $\mathbf{R}(\theta_j)$ is the rotation matrix that maps the j th link velocities from normal-tangential (v_{n_j}, v_{t_j}) to x-y coordinate (v_{x_j}, v_{y_j}) . In addition, μ_n and μ_t are the normal and tangential frictional coefficients of the grounding point, where $\mu_n \gg \mu_t$ creates anisotropic frictions enabled by passive wheels. Namely, sliding friction in the normal direction and rolling friction in the tangential direction.

3.1.1. Gait generation based on common method

The joint angles $\Psi = [\psi_1 \ \dots \ \psi_j \ \dots \ \psi_{N-1}]^T$ can track serpenoid curve $\Psi_d(t)$ via either input-output linearization based on its dynamic model, or simple model-free position controllers:

$$\mathbf{u} = \mathbf{K}(\Psi_d(t) - \Psi) \quad (4)$$

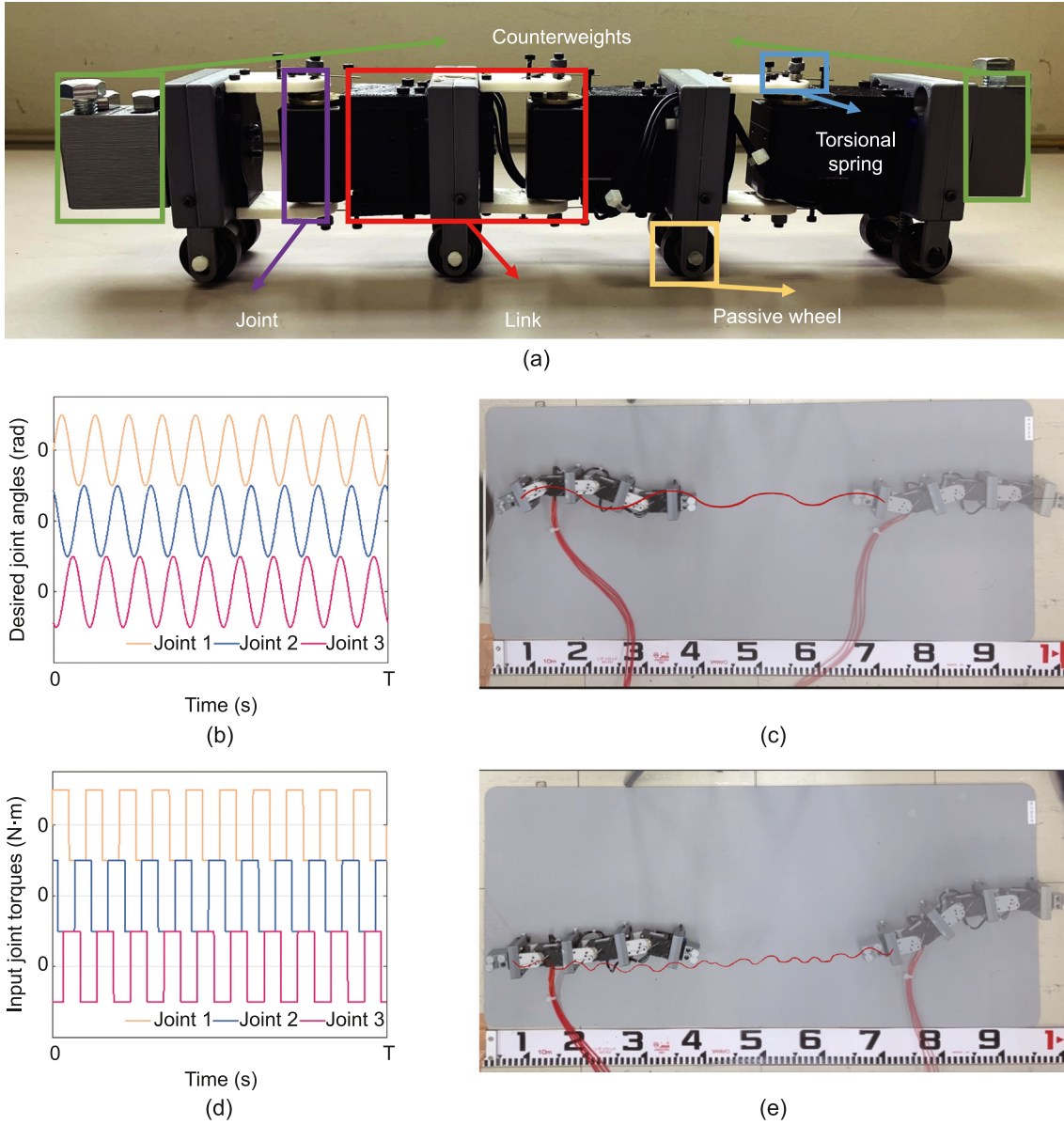


Fig. 2. Filtering behavior of undulation gait generation. (a) Experimental prototype of multi-link locomotion robot. (b-c) Angular position tracking method, and generated undulation gait. (d-e) Source filtering method, and emerged undulation gait.

where $\mathbf{K} = k\mathbf{I}_{N-1}$, k represents control gain, and \mathbf{I}_{N-1} is an identity matrix of order $N - 1$. Besides, $\Psi_d(t)$ is the simplified version of serpenoid curves [32] as shown in Fig. 1(b):

$$\Psi_d(t) = \begin{bmatrix} \psi_{1d}(t) \\ \vdots \\ \psi_{jd}(t) \\ \vdots \\ \psi_{(N-1)d}(t) \end{bmatrix} = \begin{bmatrix} A \sin(\omega t) \\ \vdots \\ A \sin(\omega t + (j - 1)\psi_\Delta) \\ \vdots \\ A \sin(\omega t + (N - 1)\psi_\Delta) \end{bmatrix} \quad (5)$$

where A is the amplitude, ω is the angular frequency, and ψ_Δ is the phase difference between neighboring joints, respectively. In addition, \mathbf{S} is the driving matrix that specifies the joint inputs

$\mathbf{S}^T \mathbf{q} = \Psi$. Accordingly, undulation gait is generated as shown in Fig. 2(c).

3.1.2. Gait generation based on source filtering method

As we observed, undulation gait, however, can also be generated based on the source filtering method. According to Eq. (4), \mathbf{u} can be separated to:

$$\mathbf{u} = \mathbf{u}_t + \mathbf{u}_k \quad (6)$$

Here,

$$\mathbf{u}_t = \mathbf{K} \Psi_d(t) \quad (7)$$

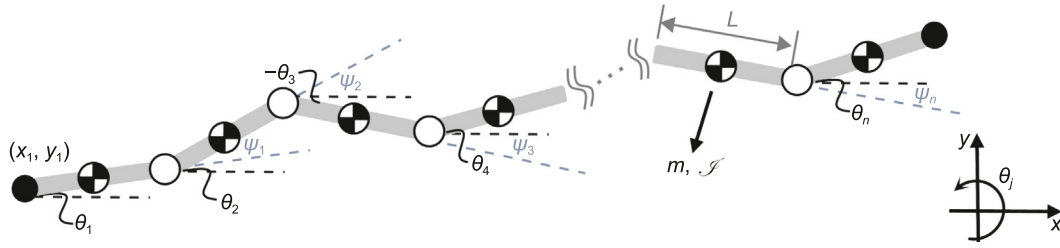


Fig. 3. A general mathematical model for multi-link locomotion robots.

becomes the open-loop torques applied on the joints, and \mathbf{K} amplifies the input signals. Besides,

$$\mathbf{u}_k = \mathbf{K}(\Psi - \Psi_n) \quad (8)$$

approximates the stiffness term of torsional springs installed on the joints, where $\Psi_n = [0 \ \cdots \ 0 \ \cdots \ 0]^T$ are equilibrium angular positions, and k becomes the spring stiffness in this sense. Note that the units of Ψ in Eqs. (4) and (7) are different. By adding a damping term \mathbf{u}_c on the joints, the revised equation of motion becomes:

$$\mathbf{M}\dot{\mathbf{q}} + \mathbf{h} = \mathbf{f} + \mathbf{S}\mathbf{u}_t + \mathbf{S}\mathbf{u}_k + \mathbf{S}\mathbf{u}_c \quad (9)$$

where

$$\mathbf{u}_c = \mathbf{C}\dot{\Psi} \quad (10)$$

$\mathbf{C} = c\mathbf{I}_{N-1}$, and c is the viscosity. Accordingly, the position controller is substituted by torsional springs and open-loop torque inputs. Moreover, the locomotion is induced by the periodical oscillation of the joints, where the oscillation is excited as follows:

$$\bar{\mathbf{I}}\ddot{\Psi} + \mathbf{C}\dot{\Psi} + \mathbf{K}\Psi = \mathbf{u}_t \quad (11)$$

Here, $\bar{\mathbf{I}} = \mathcal{I}\mathbf{I}_{N-1}$. Notably, this oscillation system can be regarded as a second-order low-pass filter of Ψ . Consequently, the open-loop torques, *i.e.*, the source injected into the filter are not necessarily harmonic, and the binary inputs shown in Fig. 2(d) are applied. According to Fig. 2(e), the sources are smoothed by the embodied filter, then generate oscillation of the joints and further produce undulation gaits.

3.2. Morphological computation

Within the framework of the source-filter theory of speech production, the morphology of the filter determines the timbre, which is roughly consistent within species yet unique across species. Accordingly, in the source-filter theory of undulation gait generation, we hypothesize that the morphology of the filter determines the gait trajectory. Consequently, morphological computation [33] is conducted based on the mathematical model introduced above to test the hypothesis, where the morphology of the robot is determined by its physical parameters, induces its mass distribution, the momentum of inertia, spring stiffness and damping. Consistent with the experimental work, binary input sources are applied. Besides, parameters listed in Table 1 are used for numerical simulation.

Table 1
Parameters for simulation.

Physical meaning	Symbol	Value	Unit
Mass	m	0.5	kg
Link length	L	0.1	m
Moment of inertia	\mathcal{I}	0.0004	kg·m ²
Gravitational acceleration	g	9.81	m/s ²
Forcing amplitude	A	1	N·m
Forcing angular frequency	ω	1	rad
Phase difference	ψ_Δ	$2\pi/3$	rad
Friction coefficient of normal direction	μ_n	0.5	-
Friction coefficient of tangential direction	μ_t	0.01	-

3.2.1. Simple example

First, we select a 4-link model and compare two conditions with respect to the morphology parameters k and c :

- High cutoff frequency condition: $k = 1$ [N·m/rad], $c = 0.2$ [N·m s/rad].
- Low cutoff frequency condition: $k = 0.05$ [N·m/rad], $c = 0.005$ [N·m·s/rad].

The numerical simulation results are shown in Fig. 4. The high cutoff frequency condition associated with high-viscoelasticity torsional springs, which corresponds to a large gain of position controller, therefore, results in a similarity between input torques (Fig. 2(d)) and the output joint angles shown in Fig. 4(a). Consequently, its locomotion trajectory shown in Fig. 4(b) is sharp.

In contrast, the low cutoff frequency condition is associated with low-viscoelasticity torsional springs, which results in harmonic-like output joint angles as shown in Fig. 4(c). Moreover, its gait trajectory shown in Fig. 4(d) is sinusoidal and highly consistent with the undulation gait generated using the common serpenoid-curve-tracking method.

3.2.2. Analysis with Fourier series

This filtering behavior can be also explained by decomposing the binary square wave via the Fourier series:

$$F_{\text{square}} = \frac{4}{\pi} \sum_{i=1}^{\infty} \frac{\sin((2i-1)\omega t)}{2i-1} \quad (12)$$

As shown in Fig. 4(e), the black wave is the original binary signal, where the amplitudes of the decomposed sine waveforms are inversely correlated with the orders. Namely, a high-order component associated with a low oscillation amplitude.

For further verification, we change the morphology parameter k from 0.05 to 1 continuously and let $c = k/10$ (neglecting the unit). After numerically generating simulation results, we eliminate the transient and decompose the joint angles of steady-state

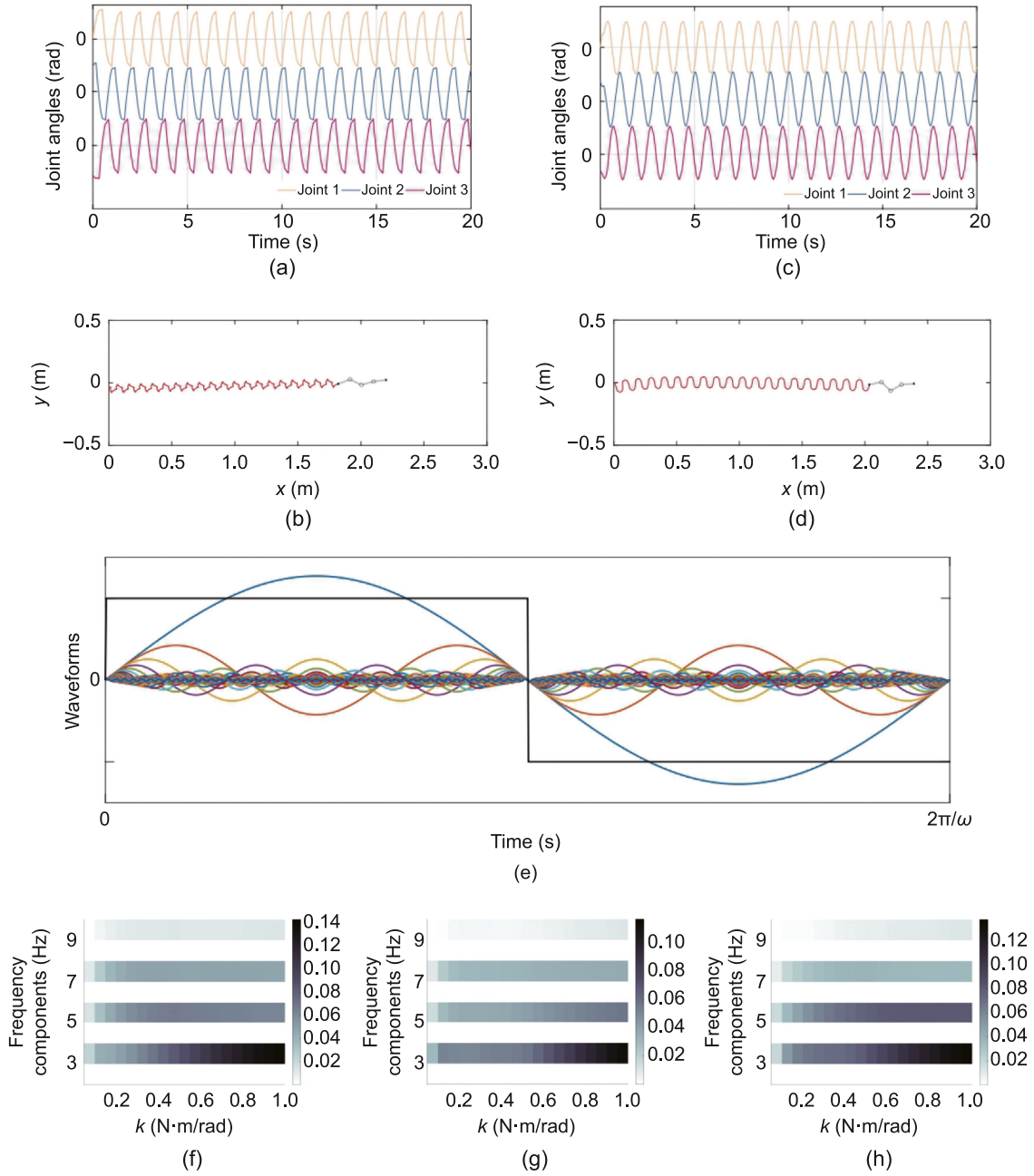


Fig. 4. Morphological computation of undulation gait of a 4-link locomotion robot generated based on source-filter theory. (a-b) generated joint angles, and gait trajectory of high cutoff frequency condition. (c-d) generated joint angles, and gait trajectory of low cutoff frequency condition. (e) Binary input decomposed by Fourier series. (f-h) Frequency components of the first, the second, and the third joint angles with respect to k , where the darker the color, the larger the amplitude of frequency component.

gait via the Fourier series. To make a convenient observation, the amplitude of all of the 1st order frequency components are normalized to 1. In Fig. 4 (f-h), we show the frequency components from the 2nd order to the 9th order, of which the amplitude is small enough. Among all cases, the even orders are in white, indicating null values, since they originally do not exist in Eq. (12). Moreover, the high-order components are much smaller than the low-orders, which is also consistent with Eq. (12) and Fig. 4(e). Moreover, the frequency components are positively correlated with k (and c), which verifies that a high-viscoelasticity of the spring provides the filter with a high cut-off frequency.

3.2.3. Embodied filter

To further investigate the embodied filter, we define input waveforms as follows:

$$\Psi_d(t) = \begin{bmatrix} A(\sin(\omega t) + \frac{\sin(\eta \omega t)}{\eta}) \\ A(\sin(\omega t) + \frac{\sin(\eta \omega t + \psi_{\Delta})}{\eta}) \\ A(\sin(\omega t) + \frac{\sin(\eta \omega t + 2\psi_{\Delta})}{\eta}) \end{bmatrix} \quad (13)$$

As shown in Fig. 5, η is varied from 2 to 10.

We use the same method introduced above to input joint torques and decompose the output joint angles concerning η . As shown in Fig. 6, the high-order components are trivial compared with the 1st order component. Nevertheless, the diagonal lines

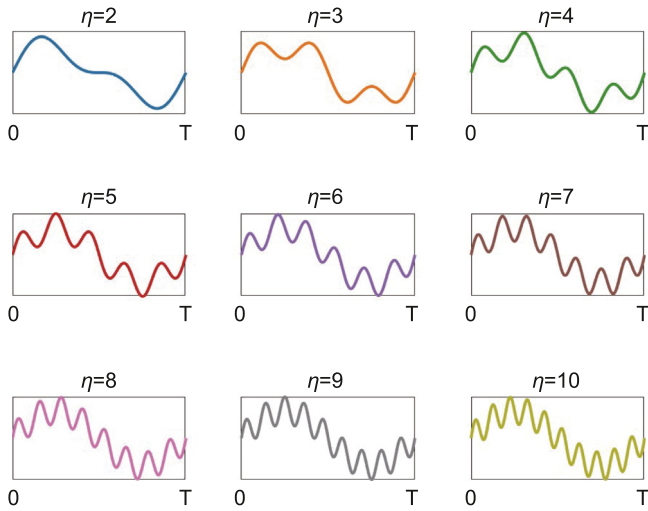


Fig. 5. Different input waveforms.

become lighter when η increases, consistent with Eq. (13). The results indicate that although the differences between input torques are significant, their output gaits are similar, since the embodied low-pass filter eliminates high-frequency components.

3.2.4. Complicate case

In the 4-link simple example, a desirable morphology can be found empirically. Then, we select an 8-link model to observe whether it becomes difficult when dealing with large link numbers. Here, two conditions with respect to the morphology parameters k and c are compared:

- High cutoff frequency condition: $k = 1$ [N·m/rad], $c = 0.2$ [N·m s/rad].
- Low cutoff frequency condition: $k = 0.05$ [N·m/rad], $c = 0.005$ [N·m·s/rad].

The numerical simulation results are shown in Fig. 7. The high cutoff frequency condition results in a similarity between input torques (Fig. 2(d)) and the output joint angles shown in Fig. 7(a). However, its locomotion trajectory shown in Fig. 4(b) does not have a concentrated direction, making circles rather than moving forward.

On the other hand, as shown in Fig. 4(c), the low cutoff frequency condition does not result in harmonic-like output joint angles. Moreover, although the locomotion direction shown in Fig. 4(d) converges eventually, its gait is unnatural and slow.

3.3. Morphology design

Last, we test the possibility of generating an undulation gait with complicated dynamics yet simple inputs. Benefiting from machine learning tools, we use the Bayesian optimization [34] method to design an appropriate morphology for the filter conveniently.

Although attaching different springs at each joint might result in better performance, we assume that a group of unified torsional springs is enough to generate a desirable undulation gait. According to Hirose’s findings [11], a periodical and smooth sinusoidal gait is not only natural but also efficient. Therefore, we eliminate the first 50 [s] dynamics of each trial, which is recognized as the transient behavior, and the smoothness of the trajectory is calculated as follows:

$$F_{smoothness} = \frac{A_{f_1}}{\sum_{i=2}^{11} A_{f_i}} \quad (14)$$

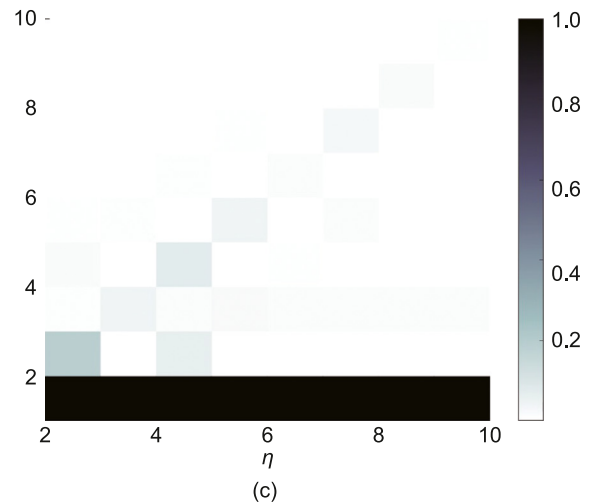
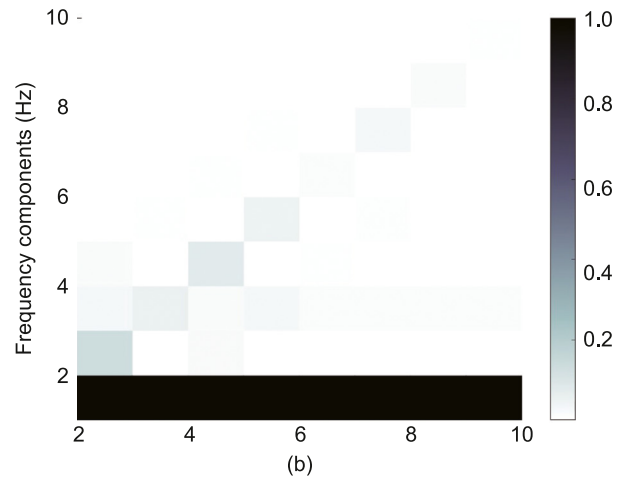
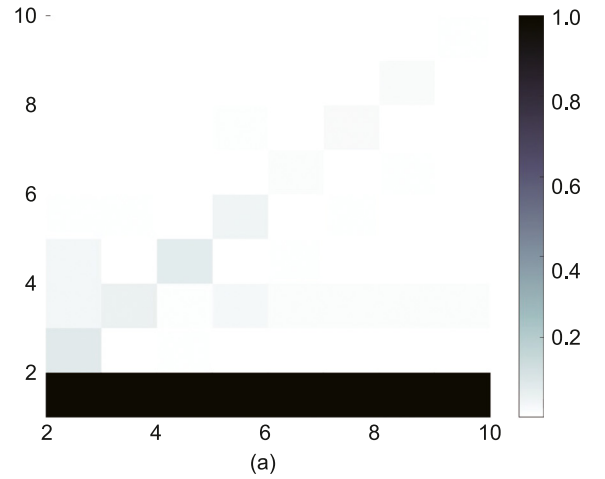


Fig. 6. Frequency components of output joint angles concerning η , where the darker the color, the larger the frequency component value. (a) The first joint. (b) The second joint. (c) The third joint.

where A_{f_i} represents the amplitude of the i th frequency component of the periodical trajectory. Namely, the smoothness is defined as the amplitude of the fundamental frequency divided by the summation from 2nd to the 11th (we assume it is enough). Consequently, a large $F_{smoothness}$ associates a large amplitude of the

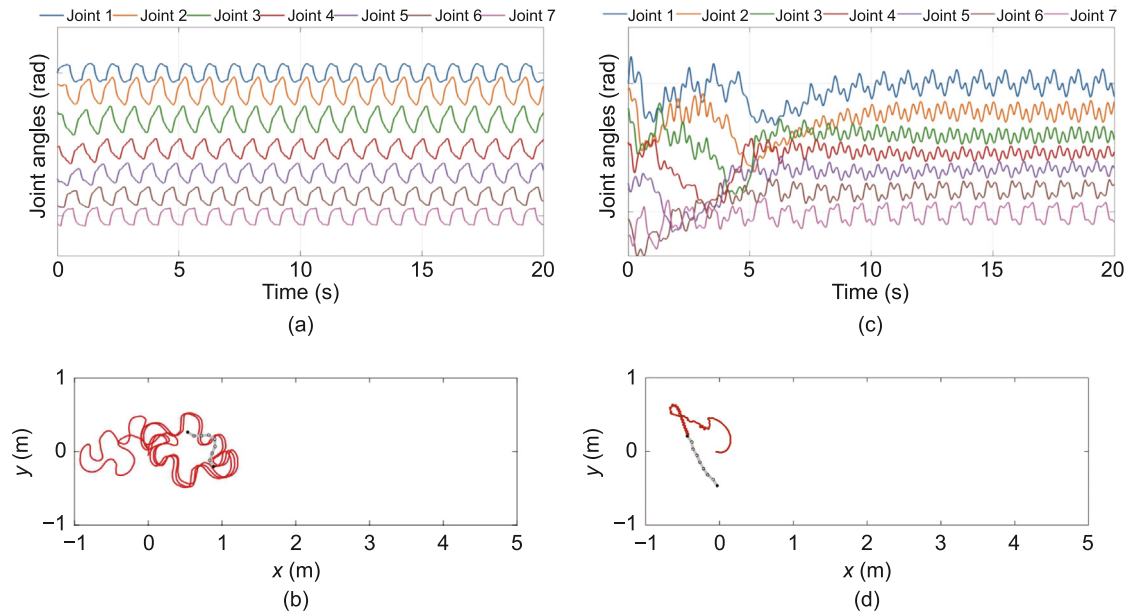


Fig. 7. Numerical results of undesirable gait of an 8-link locomotion robot generated based on source-filter theory. (a-b) generated joint angles, and gait trajectory of high cutoff frequency condition. (c-d) generated joint angles, and gait trajectory of low cutoff frequency condition.

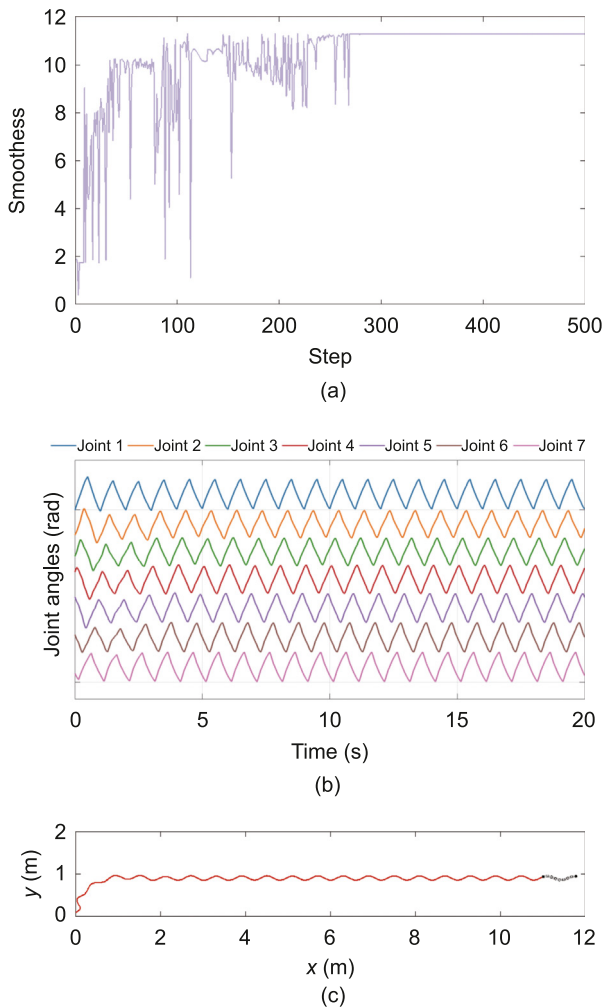


Fig. 8. Numerical results of undulation gait of an 8-link multi-link locomotion robot generated based on source-filter theory. (a) finding appropriate morphological parameters via Bayesian optimization. (b-c) generated joint angles, and gait trajectory.

fundamental frequency and small amplitudes of high-frequency components. Accordingly, one can optimize the morphology via the following process

$$\arg \max_{k, c \in \{0.01, 1\}} F_{\text{smoothness}} \quad (15)$$

where the detailed algorithm can be found in [35,36].

Fig. 8 shows the optimization process and the simulation results. The smoothness descriptor converges within 300 steps as shown in Fig. 8(a), where the optimal morphology is $k = 0.461$ [N·m/rad], $c = 0.238$ [N·m·s/rad]. Although the joint angles shown in Fig. 8(b) are triangular-like waveforms, their resultant gait trajectory is smooth, natural, and efficient, as shown in Fig. 8(c).

4. Concluding remarks

In this work, we propose a source-filter theory for undulation gait generation. Through experimental observation, numerical simulation, and theoretical analysis, one can find that by appropriately designing the morphology of the filter, undulation gait can naturally emerge with simple input sources. Consequently, our hypothesis is verified. Our work is consistent with Hunt's results [37], where a filtering behavior is observed in a jumping robot actuated by different open-loop input torques yet resulted in similar locomotion trajectories. Moreover, the importance of mechanical characteristics, *i.e.*, the passive dynamics highlighted in our work also agree with Felix's findings, where a well-designed morphology enables a plausible matching between the input sources and the embodied filter to leverage the natural dynamics of the locomotion system [38].

We further show that by increasing the complexity of the system dynamics, the importance of morphology optimization also increases. The torsional springs, on the one hand, are recognized as embodied low-pass filters that eliminate high-frequency components, which also corresponds to the control gains on the other hand. Therefore, the high-viscoelasticity of the springs corresponds to the risk of inducing shark angles of the joints, while the low-viscoelasticity of the springs corresponds to the risk of gait failure. Consequently, the balance between filter and gain is crucial for springs.

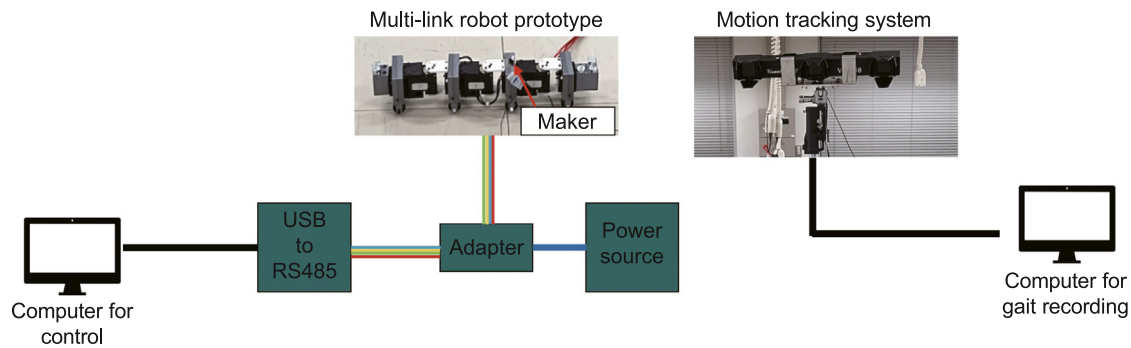


Fig. 9. Setup of gait trajectory recording experiment.

The reason we select undulation rather than other gait styles is due to the fact that this gait is general, periodic, and does not contain discrete events, unlike legged locomotion. In contrast to previous works [11], the results of morphology design indicate that generating harmonic joint angle is sufficient, yet unnecessary for enabling a sinusoidal undulation gait trajectory.

Although here we show that open-loop input torques are enough for undulation gait generation based on the proposed source-filter theory, sensory information is also important for both biological and mechanical locomotion systems. Instead of gait generation, we argue that feedback information is more important for gait transition tasks, e.g., obstacle avoidance [39], locomotion speed change [40]. Moreover, note that the filter is embodied in this work, the phase differences, however, are encoded. In contrast, it has been discussed that in biological/mechanical systems, phase differences not only can be determined via being entrained to sensory feedback [41], but also can naturally emerge based on nonlinear system dynamics via hysteresis effects [42].

The similarity between speech production and gait generation lies in their reliance on complex motor control and coordination of various body parts, regulated by the nervous system, including motor control and coordination [43,44], neurological regulation [45,46], feedback mechanisms [47,48], learning and adaptation [49,50], rhythmic patterns [51,52], and muscle activation [53,54]. These similarities highlight the intricate nature of motor control and the importance of neural regulation in both speech production and gait generation. As a starting point, our work emphasizes the importance of optimizing the morphology rather than control in periodical locomotion generation. This is more crucial in soft robots, which have more degrees of freedom yet more simple actuation [55,56], and thus rely more on their passive dynamics. To allow for resonance tuning [57] to further appropriately excite the system, different kinds of spring morphology design will be considered in our future work [31, 58]. Extending this theory to more general conditions is also of interest.

CRedit authorship contribution statement

Longchuan Li: Writing – original draft, Validation, Supervision, Methodology, Investigation. **Shugen Ma:** Writing – review & editing. **Isao Tokuda:** Writing – review & editing, Supervision. **Zaiyang Liu:** Validation. **Zhenxuan Ma:** Validation, Data curation. **Yang Tian:** Data curation. **Shuai Kang:** Writing – review & editing, Funding acquisition.

Declaration of competing interest

The authors declare that they have no known competing financial interests or personal relationships that could have appeared to influence the work reported in this paper.

Acknowledgments

This work was supported by Fundamental Research Funds for the Central Universities, China (ZY2301, BH2316, buctrc202215), the National Natural Science Foundation of China (62273340), and the Natural Science Foundation of China Liaoning Province (2021-MS-031).

Appendix A

Fig. 9 illustrates the setup of the experiments. The robot was controlled by signals sent from a Linux computer through a USB communication converter called U2D2. Motors are powered by a 12 V power source. Both the U2D2 and the power source are connected to the robot through U2D2 Power Hub. Simultaneously, the locomotion trajectory is measured by a motion-tracking system.

Appendix B. Supplementary data

Supplementary material related to this article can be found online at <https://doi.org/10.1016/j.birob.2024.100173>. This video compares the undulation gaits of a snake-like robot generated using different methods.

References

- [1] M.H. Dickinson, C.T. Farley, R.J. Full, M.A.R. Koehl, R. Kram, S. Lehman, How animals move: An integrative view, *Science* 288 (5463) (2000) 100–106.
- [2] D.M. Woolley, Evidence for twisted plane undulations in golden hamster sperm tails, *J. Cell Biol.* 75 (3) (1977) 851–865.
- [3] J. Gray, H.W. Lissmann, The locomotion of nematodes, *J. Exp. Biol.* 41 (1) (1964) 135–154.
- [4] Z.V. Guo, L. Mahadevan, Limbless undulatory propulsion on land, *Proc. Natl. Acad. Sci.* 105 (9) (2008) 3179–3184.
- [5] G.B. Gillis, Environmental effects on undulatory locomotion in the American eel *Anguilla rostrata*: Kinematics in water and on land, *J. Exp. Biol.* 201 (7) (1998) 949–961.
- [6] H. Ohno, S. Hirose, Study on slime robot (proposal of slime robot and design of slim slime robot), in: *Proceedings of the IEEE/RSJ International Conference on Intelligent Robots and Systems*, vol. 3, 2000, pp. 2218–2223.
- [7] S. Ma, H. Araya, L. Li, Development of a creeping snake-robot, in: *Proceedings of the IEEE International Symposium on Computational Intelligence in Robotics and Automation*, 2001, pp. 77–82.
- [8] H. Yamada, S. Chigisaki, M. Mori, Development of amphibious snake-like robot ACM-R5, in: *Proceedings of the 36th International Symposium on Robotics*, 2005.
- [9] A.A. Transeth, P. Liljebäck, K.Y. Pettersen, Snake robot obstacle aided locomotion: An experimental validation of a non-smooth modeling approach, in: *Proceedings of the IEEE/RSJ International Conference on Intelligent Robots and Systems*, 2007, pp. 2582–2589.
- [10] M. Porez, F. Boyer, A.J. Ijspeert, Improved lighthill fish swimming model for bio-inspired robots: Modeling, computational aspects and experimental comparisons, *Int. J. Robot. Res.* 33 (10) (2014) 1322–1341.
- [11] S. Hirose, *Biologically Inspired Robots*, Oxford Univ. Press, London, U.K., 1993.

- [12] S. Ma, Analysis of creeping locomotion of a snake-like robot, *Adv. Robot.* 15 (2) (2001) 205–224.
- [13] Z. Wang, S. Ma, B. Li, Y. Wang, Passive creeping of a snake-like robot, in: *Proceedings of the IEEE International Conference on Robotics and Biomimetics*, 2009, pp. 57–62.
- [14] D. Chen, Z. Wu, H. Dong, M. Tan, J. Yu, Exploration of swimming performance for a biomimetic multi-joint robotic fish with a compliant passive joint, *Bioinspir. Biomim.* 16 (2) (2020) 026007.
- [15] Y. Cao, L. Li, S. Ma, A creeping snake-like robot with partial actuation, in: *Proc. 2022 IEEE/RSJ International Conference on Intelligent Robots and Systems, IROS 2022*, 2022, pp. 1202–1207.
- [16] L. Li, S. Ma, I. Tokuda, Y. Tian, Y. Cao, M. Nokata, Z. Li, Embodying rather than encoding: Undulation with binary input, in: *Proc. 2022 IEEE/RSJ International Conference on Intelligent Robots and Systems, IROS 2022*, 2022, pp. 1196–1201.
- [17] T. Chiba, M. Kajiyama, *The Vowel: Its Nature and Structure*, Phonetic society of Japan, Tokyo, 1958.
- [18] G. Fant, T. Chiba, M. Kajiyama, Pioneers in speech acoustics ((feature articles) sixtieth anniversary of the publication of the vowel, its nature and structure by Chiba and Kajiyama), *J. Phonet. Soc. Japan* 5 (2) (2001) 4–5.
- [19] Isao T. Tokuda, The source/filter theory of speech, in: *The Oxford Research Encyclopedia of Linguistics*, 2021.
- [20] A.M. Taylor, D. Reby, The contribution of source–filter theory to mammal vocal communication research, *J. Zool.* 280 (3) (2010) 221–236.
- [21] Isao T. Tokuda, Non-linear dynamics in mammalian voice production, *Anthropol. Sci.* 126 (1) (2018) 35–41.
- [22] Y. Li, J. Li, M. Akagi, Contributions of the glottal source and vocal tract cues to emotional vowel perception in the valence-arousal space, *J. Acoust. Soc. Am.* 144 (2) (2018) 908–916.
- [23] T. Saitou, M. Unoki, M. Akagi, Development of an F0 control model based on F0 dynamic characteristics for singing-voice synthesis, *Speech Commun.* 46 (3–4) (2005) 405–417.
- [24] X. Wang, S. Takaki, J. Yamagishi, Neural source-filter-based waveform model for statistical parametric speech synthesis, in: *ICASSP 2019-2019 IEEE International Conference on Acoustics, Speech and Signal Processing, ICASSP, 2019*, pp. 5916–5920.
- [25] A. Rao, P.K. Ghosh, SFNet: A computationally efficient source filter model based neural speech synthesis, *IEEE Signal Process. Lett.* 27 (2020) 1170–1174.
- [26] T. McGeer, Passive dynamic walking, *Int. J. Robot. Res.* 9 (2) (1990) 62–82.
- [27] R. Pfeifer, M. Lungarella, F. Iida, Self-organization, embodiment, and biologically inspired robotics, *Science* 318 (2007) 1088–1093.
- [28] P.E. Schiebel, J.M. Rieser, A.M. Hubbard, L. Chen, D.Z. Rocklin, D.I. Goldman, Mechanical diffraction reveals the role of passive dynamics in a slithering snake, *Proc. Natl. Acad. Sci.* 116 (11) (2019) 4798–4803.
- [29] D.N. Beal, F.S. Hover, M.S. Triantafyllou, J.C. Liao, G.V. Lauder, Passive propulsion in vortex wakes, *J. Fluid Mech.* 549 (2006) 385–402.
- [30] T. Dear, B. Buchanan, R. Abrájan-Guerrero, S.D. Kelly, M. Travers, H. Choset, Locomotion of a multi-link non-holonomic snake robot with passive joints, *Int. J. Robot. Res.* 39 (5) (2020) 598–616.
- [31] A. Kakogawa, S. Jeon, S. Ma, Stiffness design of a resonance-based planar snake robot with parallel elastic actuators, *IEEE Robot. Autom. Lett.* 3 (2) (2018) 1284–1291.
- [32] M. Tesch, K. Lipkin, I. Brown, R. Hatton, A. Peck, J. Rembisz, H. Choset, Parameterized and scripted gaits for modular snake robots, *Adv. Robot.* 23 (9) (2009) 1131–1158.
- [33] H. Hauser, A.J. Ijspeert, R.M. Fuchsln, R. Pfeifer, W. Maass, Towards a theoretical foundation for morphological computation with compliant bodies, *Biol. Cybern.* 105 (5) (2011) 355–370.
- [34] J. Snoek, H. Larochelle, R.P. Adams, Practical Bayesian optimization of machine learning algorithms, in: *Advances in Neural Information Processing Systems*, vol. 25, 2012.
- [35] K.A. Saar, A. Rosendo, F. Iida, Bayesian optimization of gaits on a bipedal slip model, in: *2017 IEEE International Conference on Robotics and Biomimetics, ROBIO, 2017*, pp. 1812–1817.
- [36] K.A. Saar, F. Giardina, F. Iida, Model-free design optimization of a hopping robot and its comparison with a human designer, *IEEE Robot. Autom. Lett.* 3 (2) (2018) 1245–1251.
- [37] J. Hunt, F. Giardina, A. Rosendo, F. Iida, Improving efficiency for an open-loop-controlled locomotion with a pulsed actuation, *IEEE/ASME Trans. Mechatronics* 21 (3) (2016) 1581–1591.
- [38] F. Ruppert, A. Badri-Spröwitz, Learning plastic matching of robot dynamics in closed-loop central pattern generators, *Nat. Mach. Intell.* 4 (7) (2022) 652–660.
- [39] P. Liljebäck, K.Y. Pettersen, Ø. Stavdahl, J.T. Gravdahl, Snake robot locomotion in environments with obstacles, *IEEE/ASME Trans. Mechatronics* 17 (6) (2011) 1158–1169.
- [40] X. Wu, S. Ma, Adaptive creeping locomotion of a CPG-controlled snake-like robot to environment change, *Auton. Robots* 28 (3) (2010) 283–294.
- [41] R. Thandiackal, K. Melo, L. Paez, J. Herault, T. Kano, K. Akiyama, A.J. Ijspeert, Emergence of robust self-organized undulatory swimming based on local hydrodynamic force sensing, *Science Robotics* 6 (57) (2021) eabf6354.
- [42] L.C. van Laake, J. de Vries, S.M. Kani, J.T.B. Overvelde, A fluidic relaxation oscillator for reprogrammable sequential actuation in soft robots, *Matter* 5 (9) (2022) 2898–2917.
- [43] R.D. Kent, Research on speech motor control and its disorders: A review and prospective, *J. Commun. Disorders* 33 (5) (2000) 391–428.
- [44] D.A. Winter, Human balance and posture control during standing and walking, *Gait Posture* 3 (4) (1995) 193–214.
- [45] S. Grillner, Neurobiological bases of rhythmic motor acts in vertebrates, *Science* 228 (4696) (1985) 143–149.
- [46] S. Grillner, Control of Locomotion in Biped, Tetrapods, and Fish, in: *Handbook of Physiology: The Nervous System II*, pp. 1179–1236.
- [47] J.A. Tourville, F.H. Guenther, The DIVA model: A neural theory of speech acquisition and production, *Lang. Cogn. Process.* 26 (7) (2011) 952–981.
- [48] A. Shumway-Cook, M.H. Woollacott, *Motor Control: Translating Research Into Clinical Practice*, Lippincott Williams and Wilkins, 2007.
- [49] D.M. Wolpert, J. Diedrichsen, J.R. Flanagan, Principles of sensorimotor learning, *Nat. Rev. Neurosci.* 12 (12) (2011) 739–751.
- [50] V. Dietz, Human neuronal control of automatic functional movements: Interaction between central programs and afferent input, *Physiol. Rev.* 72 (1) (1992) 33–69.
- [51] R.B. Ivry, R.E. Hazeltine, Perception and production of temporal intervals across a range of durations: Evidence for a common timing mechanism, *J. Exp. Psychol.: Hum. Percept. Perform.* 21 (1) (1995) 3–18.
- [52] J.M. Hausdorff, et al., Gait variability and basal ganglia disorders: Stride-to-stride variations of gait cycle timing in Parkinson's disease and Huntington's disease, *Movement Disorders* 13 (3) (1996) 428–437.
- [53] A.A. Smith, The control of voluntary speech movements, *J. Acoust. Soc. Am.* 92 (2) (1992) 739–755.
- [54] K. Takakusaki, Functional neuroanatomy for posture and gait control, *J. Mov. Disord.* 10 (1) (2017) 1–17.
- [55] D.Q. Nguyen, V.A. Ho, Anguilliform swimming performance of an eel-inspired soft robot, *Soft Robot.* 9 (3) (2022) 425–439.
- [56] L. Li, C. Zhao, S. He, Q. Qi, S. Kang, S. Ma, Enhancing undulation of soft robots in granular media: A numerical and experimental study on the effect of anisotropic scales, *Biomimetic Intell. Robot.* 4 (2) (2024) 100158.
- [57] L. Li, S. Ma, I. Tokuda, F. Asano, M. Nokata, Y. Tian, L. Du, Generation of efficient rectilinear gait based on dynamic morphological computation and its theoretical analysis, *IEEE Robot. Autom. Lett.* 6 (2) (2021) 841–848.
- [58] A. Kakogawa, T. Kawabata, S. Ma, Plate-springed parallel elastic actuator for efficient snake robot movement, *IEEE/ASME Trans. Mechatronics* 26 (6) (2021) 3051–3063.